

Practical learning method for multi-scale entangled states

Olivier Landon-Cardinal and David Poulin

Département de Physique, Université de Sherbrooke, Sherbrooke, Québec, J1K 2R1, Canada

We describe a method for reconstructing multi-scale entangled states from a small number of efficiently-implementable measurements and fast post-processing. The method only requires single-particle measurements and the total number of measurements is polynomial in the number of particles. Data post-processing for state reconstruction uses standard tools, namely matrix diagonalisation and conjugate gradient method, and scales polynomially with the number of particles. Our method prevents the build-up of errors from both numerical and experimental imperfections.

I. INTRODUCTION

Quantum state tomography [1] is a method to learn a quantum state from measurements performed on many identically prepared systems. This task is crucial not only to assess the degree of control exhibited during the preparation and transformation of quantum states, but also in comparing theoretical predictions to real-life systems. For instance, numerical methods are used to compute the ground states or thermal states of model quantum systems. Quantum state tomography could be used to check that the experimental state corresponds to the predicted one, thus providing an essential link between theory and experiments. For example, one could in principle use tomography to settle the question [2] of which states correctly describe the quantum Hall fluid at various filling parameters.

In practice however, the state of n particles is described by a number of parameters that scales exponentially with n . Therefore, tomography requires an exponential number of identically prepared systems on which to perform exponentially many measurements needed to span a basis of observables that completely characterizes the state. Furthermore, solving the inference problem to determine the quantum state that is compatible with all these measurement outcomes requires an exponential amount of classical post-processing. These factors limit tomography to at most a few tens of particles.

While this is unavoidable for a generic state, many states encountered in nature have special properties that could be exploited to simplify the task of tomography. In fact, the overwhelming majority of tomographic experiments performed to date [3–9] were used to learn state described with only a few parameters. Such variational states—family of states specified with only a few parameters—are widespread in many-body physics because they are tailored for numerical calculations and can predict many phenomena observed in nature (Kondo effect, superconductivity, fractional statistics, etc). One example, familiar to the quantum information community, is matrix product states (MPS) [10–13] that are at the heart of the density matrix renormalisation group (DMRG) numerical method, suitable for the description of one-dimensional quantum systems with finite correlation length [14].

Recently, we and others have demonstrated [15] that

tomography can be performed efficiently on MPS, *i.e.*, such states can be learned from a small number of simple measurements and efficient classical post-processing. Here, we take this result one step further and demonstrate that it is possible to efficiently learn the states associated to the multi-scale renormalization ansatz (MERA) introduced by Vidal [16], for which efficient numerical algorithms to minimize the energy of local Hamiltonians exist [17]. As opposed to MPS, these MERA states are not restricted to one dimension and can describe systems with long-range correlation. This last distinction is important because one of the most interesting phenomena in physics, quantum phase transitions, leads to a diverging correlation length and are therefore not suitably described by MPS. In contrast, MERA have been successfully used to study numerous many-body models, such as the critical Ising model in 1D [17] and 2D [18], and can also accurately describe systems with topological order [19–24].

In this work, we present two related methods to learn the one-dimensional MERA description of a state using tomographic data obtained from local measurements performed on several copies of the states. Our learning methods for MERA are based on the identification of the unitary gates in the quantum circuit that outputs the MERA state. In that regard, this Article is a continuation of our work on MPS and is reminiscent of early methods to numerically optimise MERA tensors [25]. However, going from MPS to MERA is non-trivial because MERA exhibits a spatial arrangement of gates that is more elaborate. Since MERA is a powerful numerical tool, our learning method bridges the gap between numerical simulations and experiments by allowing the direct comparison of numerical predictions to experimental states.

The first method we present requires unitary control of the system and the ability to perform tomography on blocks of a few particles, which can be realized using the correlations between single-particle measurements. Crucially, the size of those blocks does not depend on the total size of the system, making it a *scalable* method. In an experiment, one cannot know beforehand if the state in the lab is a MERA. However, our method contains a built-in certification procedure from which one can assess the proper functioning of the method as the experiments are performed and conclusively determine if the state is

well described by the MERA. The second method builds on the first one, but completely circumvents the need for unitary control. Thus, this MERA learning method can be implemented with existing technologies. The drawback of this simplified method is that it does not come with a built-in certification procedure. Certification in this case can be realized using the Monte Carlo scheme [26], which requires the same experimental toolbox.

The rest of the paper is organised as follows. We first present the proposed method for MERA learning in section II. Subsection II A explains how to identify the disentanglers. We start by deriving a necessary condition for the existence of suitable disentangler and then turn this criterion into a heuristic objective function that we minimize numerically over unitary space. In subsection II B, we carefully analyze the buildup of errors in our procedure and show that errors only accumulate linearly with the size of the system. In subsection II C, we present numerical benchmarks of our tomography method. In subsection, II D, we present the simplified method by demonstrating that it is not necessary to apply the disentanglers to the experimental state since we can simulate the effect of those disentanglers numerically, albeit at the cost of more repeated measurements and a slightly worse error scaling (analyzed in appendix A). In section III, we discuss potential issues for our numerical scheme and suggest modifications to prevent them. Finally, we present in appendix B a tool to contract two different MERA states, which allows for the efficient comparison of a MERA whose parameters have been identified experimentally using our method to a predicted theoretical MERA state.

II. MERA LEARNING

A. Identifying the disentanglers

MERA states can be described as the output of a quantum circuit [16] whose structure is represented on Fig. 1 (as seen with inputs on the top and output at the bottom). For simplicity, we will focus on a one dimensional binary MERA circuit for qubits, but our method generalizes to all 1D MERA states, *i.e.*, particles could have more internal states thus accounting for a larger MERA refinement parameter χ and isometries could renormalize several particles to one effective particle. The circuit contains three classes of unitaries. Disentanglers (represented as \square) are two-qubit unitary gates; isometries (represented as \triangle) are also two-qubit gates but with one input qubit always in the $|0\rangle$ state; the top tensor (represented as \circ) is a special case of isometry that takes as input two qubits in the $|00\rangle$ state. Each renormalisation layer is made of a row of disentanglers and a row of isometries. Disentanglers remove the short-scale entanglement between adjacent blocks of two qubits while isometries renormalise each pair of qubits to a single qubit. Each renormalisation layer performs these operations on a dif-

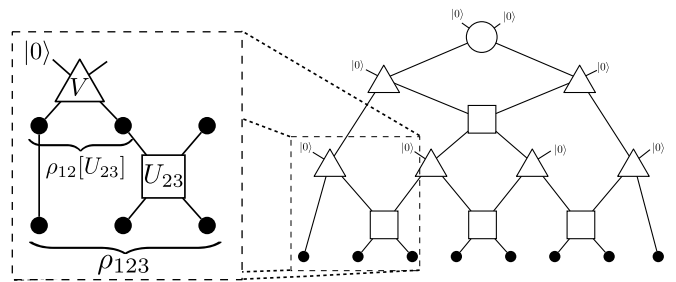


Figure 1: The optimal disentangler \tilde{U} can be computed from the tomographic estimation of the density matrix ρ_{123} on the first three qubits. Once applied, the resulting state $\tilde{\rho}_{12}[\tilde{U}]$ is very close to a rank 2 matrix. Thus, there exist a unitary V such that $\tilde{\rho}_{12}[\tilde{U}]$ can be rotated such that the first qubit is almost in the state $|0\rangle$.

ferent lengthscale. The quantum circuit thus mirrors the renormalisation procedure that underlies the MERA.

Learning a MERA amounts to identifying the various gates in that circuit, which turns the experimental state into the all $|0\rangle$ state. The intuitive idea behind our scheme is to proceed by varying the isometries and disentanglers until the “ancillary” qubits reach the state $|0\rangle$ for each row of isometries. We will exploit this feature to numerically determine each disentangler.

1. Necessary condition for disentangler

Consider the n qubits at the lowest layer of the MERA. Let ρ_{123} be the reduced density matrix on the three first qubits (see Fig. 1). If the state is exactly a MERA, there exists a unitary U_{23} acting on qubits 2 and 3 (see left of Fig. 1) such that applying this unitary and tracing out the 3rd qubit yields a density matrix

$$\rho_{12}[U_{23}] = \text{Tr}_3 \left[\left(\mathbb{I}_1 \otimes U_{23} \right) \rho_{123} \left(\mathbb{I}_1 \otimes U_{23}^\dagger \right) \right] \quad (1)$$

of rank at most 2. Indeed, if the rank was strictly greater than 2, it would be impossible for the isometry V (see left of Fig. 1) to map the density matrix $\rho_{12}[U_{23}]$ to a state with one of the qubit in the state $|0\rangle$ because the dimension of the space $|0\rangle \otimes \mathbb{C}^2$ would be strictly smaller than the dimension of the support of the density matrix. Hence, we have the necessary criterion

$$\exists \tilde{U}_{23} \quad \rho_{12}[\tilde{U}_{23}] \text{ has rank less or equal than 2.} \quad (2)$$

To find a unitary that fulfills this criterion, it is necessary to know the state ρ_{123} , and this can be achieved by brute-force tomography on these three qubits. Once the original state on the three qubits is known, one has to perform a search over the space of unitaries to find a suitable disentangler. To do this, we will define an objective function to minimise numerically.

Once this optimal unitary operator \tilde{U} has been found numerically, it is necessary to consider how it modifies the

quantum state before learning the other elements of the circuit. One obvious way to do so is to apply the unitary transformation to the experimental state and continue the procedure on the transformed state. This amounts to undoing the circuit, and should in the end map the experimental state to the all $|0\rangle$ state. For simplicity, we will first present our scheme assuming that the state is transformed at every step this way. Of course, such unitary control increases the complexity of the scheme and could be out of the reach of current technologies. However, in section IID, we will explain how this unitary transformation can be circumvented at the cost of a slight increase in the number of measurements.

After the optimal disentangler \tilde{U} has been applied to the state, we need to identify the unitary V that rotates the density matrix on the first two qubits such that the first qubit is brought to the $|0\rangle$ state, c.f. Fig 1 left. This does not require any additional tomographic estimate since we already know the descriptions of the state on the three first qubits and the disentangler. We can thus compute the state on the first two qubits $\rho_{12}[\tilde{U}]$ and diagonalise it to obtain the eigenvectors corresponding to its two non-zero eigenvalues. The unitary V is chosen to map those two eigenvectors to the space $|0\rangle \otimes \mathbb{C}^2$, i.e., V rotates the qubits such that the support of the density matrix is mapped to a space where the first qubit is in the $|0\rangle$ state.

All other disentanglers of this layer can be found by recursing the above procedure. Once a disentangler has been identified, it is physically applied to the system and brute-force tomography is performed on the next block of three qubits.

Notice that for the last block, a single unitary is responsible for minimising the rank of two density matrices, $\rho_{n-3,n-2}$ and $\rho_{n-1,n}$. One possible way to handle this is to get a tomographic estimate of the state on the last four qubits and to try to minimise the rank of both reduced matrices. Another way, for which we have opted in our numerical simulations, is to perform multiple sweeps over the layer. For instance, the disentanglers will first be identified from left to right and then the next sweep will be performed from right to left, using the disentanglers found in the first sweep as initial guesses in the space of unitaries (see Fig. 2). The number of sweeps can be increased for better accuracy but each additional sweep requires to extract the tomographic estimates again. Multiple sweeps would also allow to apply our method to MERA states with periodic boundary conditions in 1D and could be useful for 2D-MERA states. While this would be an interesting continuation of our work, we focus on 1D-MERA for the rest of the article.

2. Heuristic objective functions

One of the steps in our protocol consists in identifying the unitary \tilde{U} that minimizes the rank of $\rho_{12}[U]$, c.f. eq. (1). There are many distinct ways this can be done

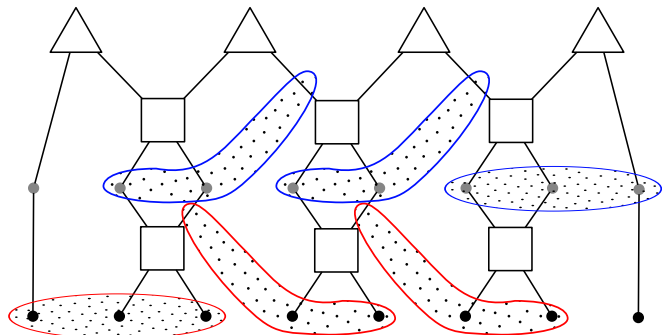


Figure 2: Identification of the disentanglers using two successive sweeps of the chain. Dotted regions cover particles on which brute-force tomography is performed. The first sweep (red dotted regions) finds unitaries starting from the left end of the chain. Those unitaries will be used as initial guesses for the second sweep (blue striped regions) that starts from the right end of the chain.

and in this section, we present a practical heuristic to accomplish this task. Minimising the rank of the density matrix $\rho_{12}[U]$ is not a suitable numerical task because, even if the experimental state is an exact MERA, the inferred density matrix will typically have full rank due to machine precision and the imperfect tomographic estimation of ρ_{123} . Thus, we turn the problem of finding \tilde{U}_{23} into an optimization problem by considering the eigendecomposition of $\rho_{12}[U] = \sum_k \lambda_k |\psi_k\rangle\langle\psi_k|$ where the eigenvalues are sorted in decreasing order $\lambda_1 \geq \lambda_2 \geq \lambda_3 \geq \lambda_4$. If $\rho_{12}[U]$ has most of its support on a two-dimensional space, it will have two small eigenvalues that are typically non-zero due to imperfections. We thus consider the objective function

$$f(U, \rho_{123}) = \sum_{k>2} \lambda_k \quad (3)$$

and we perform a minimisation over the space of unitaries to determine the optimal unitary \tilde{U} . This objective function has a well-defined operational meaning – it is the probability of measuring the disentangled qubit in the $|1\rangle$ state after the isometry V has been applied. We will see in section IIB that this property can be used to certify the distance between the experimental and the reconstructed states.

Another way to think about this objective function is to consider the characteristic polynomial $P[X]$ of $\rho_{12}[U]$ which is of the form

$$P[X] = X^4 - X^3 + aX^2 - bX + c \quad (4)$$

where the coefficients a , b and c are positive since they correspond to the sum of product of the positive eigenvalues of the density matrix. In particular, coefficient b is the sum of all products of three eigenvalues, i.e., $b = \lambda_1\lambda_2\lambda_3 + \lambda_1\lambda_2\lambda_4 + \lambda_1\lambda_3\lambda_4 + \lambda_2\lambda_3\lambda_4$. In order for the rank of the density matrix to be 2, it is sufficient for all 4 products of three eigenvalues to vanish, i.e.,

$$\rho_{12}[U] \text{ of rank less than 2} \iff b = 0. \quad (5)$$

Thus, another suitable objective function is the positive coefficient b , which is a polynomial in the entries of $\rho_{12}[U]$. Indeed, using Bocher formula, coefficient b can be expressed as $6b = 1 - 3\text{Tr}A^2 + 2\text{Tr}A^3$ where $A = \rho_{12}[U]$. Thus, b is a well-behaved function with respect to the density matrix. Note also that b can be expressed without diagonalising the density matrix $\rho_{12}[U]$. We will focus on minimising (3) in all subsequent numerical discussion and results.

3. Numerical minimisation over unitary space

Minimisations of (3) is performed using a conjugate gradient method. We first have to account for the fact that the unitary manifold is not a vector space. To get around this problem, we go to the Hermitian space by writing any unitary U as the result of a Hamiltonian evolution, *i.e.*, there exists a Hermitian matrix H such that $U = e^{iH}$. It is then possible to use the standard conjugate gradient method. Let us sketch the algorithm in more details.

First, we select a unitary U_0 either at random or from an initial guess (provided for instance by a previous sweep). We will search the unitary space by generating a sequence of unitaries $\{U_k\}$. At the k^{th} step of the minimisation, the algorithm is the following.

1. We center the unitary space at point U_{k-1} by defining $\rho_k = (\mathbb{I} \otimes U_{k-1})\rho_{k-1}(\mathbb{I} \otimes U_{k-1})^\dagger$.
2. We compute the gradient $G^{(k)}$ by parametrizing the Hamiltonian H on 2 qubits by its decomposition on the Pauli group $H = \sum_{\mu\nu} h_{\mu\nu}\sigma_\mu \otimes \sigma_\nu$ where $\sigma_\mu \in \{\mathbb{I}, \sigma_x, \sigma_y, \sigma_z\}$ is a Pauli matrix. We successively evaluate the component of the gradient $G^{(k)}$ in the direction (μ, ν) by looking at the effect of the test unitary $U_{\mu,\nu} = \mathbb{I} + i\epsilon\sigma_\mu \otimes \sigma_\nu$ on the objective function, *i.e.*, $G_{\mu,\nu}^{(k)} = \frac{f(U_{\mu,\nu}, \rho_k) - f(\mathbb{I}, \rho_k)}{\epsilon}$ where ϵ is a small number.
3. Instead of following the gradient, which would generally undo some of the minimization performed in the previous steps, we use a conjugate gradient method where the new direction of search $\tilde{G}^{(k)}$ is optimized by taking into account the direction used in the previous step $\tilde{G}^{(k-1)}$ through the Polak-Ribière formula. More precisely, $\tilde{G}^{(k)} = G^{(k)} + \beta\tilde{G}^{(k-1)}$ in which the real parameter β is defined as $\beta = \max\left(0, \frac{G^{(k)} \cdot (\tilde{G}^{(k-1)} - G^{(k)})}{\tilde{G}^{(k-1)} \cdot \tilde{G}^{(k-1)}}\right)$.
4. We perform a line search along the direction $\tilde{G}^{(k)}$ by considering the family of unitaries $\exp\left(-it \sum_{\mu,\nu} \tilde{G}_{\mu,\nu} \sigma_\mu \otimes \sigma_\nu\right)$ and optimizing the parameter t to find t_{opt} . We then define

$$U_k = \exp\left(-it_{opt} \sum_{\mu,\nu} \tilde{G}_{\mu,\nu} \sigma_\mu \otimes \sigma_\nu\right) U_{k-1} \quad (6)$$

which ends the k^{th} iteration.

We iterate until the objective function is close enough to zero or that improvement has stopped.

This method is *heuristic* since the objective functions present no characteristic that would ensure the convergence of the conjugate gradient method. In particular, our search over unitary space depends on the starting point, *i.e.*, the unitary chosen in the first iteration. Indeed, some starting points will lead the heuristic to a local minima where it will get stuck. In order to avoid this phenomenon, we can repeat the overall search by picking at random (according to the unitary Haar measure) different initial points which lead to potentially different minima and keep the smallest of those minima, which we expect to be the global minimum. In any case, this is a minimization problem over a space of *constant* dimension, so the method used to solve it does not affect the scaling with the number of particles n . Ultimately, we can always use a finite mesh over the unitary space and use brute-force search. Nevertheless, we found numerically that this heuristic works well.

It is also possible that a choice of unitary that is optimal locally, in the sense that it minimizes (3), is not optimal globally as it might lead to a state for which it is impossible to find a disentangler obeying (3) elsewhere in the circuit. This is a phenomenon that is more likely to occur when the minimum is degenerate, *i.e.*, there exists several distinct (modulo gauge) exact disentanglers for the state. However, we have performed numerical experiments on randomly generated MERA states as well as physically motivated states and found that the conjugate gradient performs well (see section II C).

B. Error analysis

In practice, due to numerical and experimental imperfections, the disentangled qubits will not be exactly in the $|0\rangle$ state, but merely close to it. This situation arises from the conjunction of three causes : *i*) the experimental state of the system is not exactly a MERA, but merely close to one, *ii*) the tomographic estimate of the density matrices on blocks of three qubits are slightly inaccurate due to noisy measurements and experimental finite precision, *iii*) the numerical minimization did not find the exact minimum.

1. Isolating each elementary steps to prevent error buildup

Our error analysis will show that the buildup of errors is linear in the number of disentanglers of the MERA circuit which is itself linearly proportional to the number of particles in the experimental state. Essentially, the distance between the reconstructed state and the experimental state is the sum of the error made at each elementary step when estimating a disentangler and an

isometry. Fortunately, the error made at each elementary step does not depend on the errors made at previous steps. The key to isolate each step from the others is to measure the qubit that should have been disentangled in the computational basis. With high probability the qubit will be found in the $|0\rangle$ state. While the probability of measuring the $|0\rangle$ outcome depends on previous errors, the post-selected state is now free from previous errors. The interest of this postselection is two-fold. First, it forbids errors in previous steps to contaminate the state and amplify the error made at the current step, thus limiting the error propagation. Second, by accumulating statistics on this measurement, we can estimate the probability of the all-0 outcome and use it to bound the distance of the reconstructed state to the actual state in the lab. Therefore, our procedure comes with a *built-in certification process*. Let us now describe the error analysis in more details.

2. Error at each elementary step

Recall the notation of Fig. 1. Due to numerical and experimental imperfections, the state on qubits 1, 2 and 3 after applying the disentangler \tilde{U}_1 and the isometry V_1 is not exactly in the $|0\rangle \otimes \mathbb{C}^{2(n-1)}$ subspace but contains a small component orthogonal to that space. Thus, it has the form

$$V_1 \tilde{U}_1 |\psi\rangle = \frac{|0\rangle |\eta_1\rangle + |e_1\rangle}{\sqrt{1 + \langle e_1 | e_1 \rangle}} \quad (7)$$

where $|\eta_1\rangle$ is the normalised pure state on qubits 2 to n if qubit 1 had been completely disentangled from the chain and $|e_1\rangle$ is some *subnormalized* vector supported on the subspace $|1\rangle \otimes \mathbb{C}^{2(n-1)}$. The isometry V_1 is chosen to minimize the norm of $|e_1\rangle$, i.e., to minimize $\epsilon_1 \equiv \langle e_1 | e_1 \rangle$.

Further along the layer, the state after applying k disentanglers and k isometries will be of the form

$$V_k \tilde{U}_k \dots V_1 \tilde{U}_1 |\psi\rangle = \frac{|0\rangle^{\otimes k} |\eta_k\rangle + |e_k^{cm}\rangle}{\sqrt{1 + \epsilon_k^{cm}}} \quad (8)$$

where the first term $|0\rangle^{\otimes k} |\eta_k\rangle$ is the normalised state had the k qubits in position 1, 3, ..., $2k-3$ been completely disentangled from the chain and $|e_k^{cm}\rangle$ is the accumulated error vector orthogonal to the space where those k qubits are in the $|0\rangle^{\otimes k}$ state. In order to find the optimal disentangler and isometry, we measure the last disentangled qubit in the computational basis and post-select on the $|0\rangle$ outcome, which occurs with probability $(1 + \epsilon_k^{cm})^{-1}$. We then perform brute force tomography and identify numerically the disentangler and the isometry that minimizes the norm of the error vector $|e_{k+1}\rangle$ such that

$$V_{k+1} \tilde{U}_{k+1} |\eta_k\rangle = \frac{|0\rangle |\eta_{k+1}\rangle + |e_{k+1}\rangle}{\sqrt{1 + \epsilon_{k+1}}}. \quad (9)$$

Applying this disentangler and isometry to the whole state of the chain, one gets

$$V_{k+1} \tilde{U}_{k+1} \dots V_1 \tilde{U}_1 |\psi\rangle = \frac{|0\rangle^{\otimes k+1} |\eta_{k+1}\rangle + |e_{k+1}^{cm}\rangle}{\sqrt{1 + \epsilon_{k+1}^{cm}}} \quad (10)$$

where the accumulated error vector at step $k+1$ is

$$|e_{k+1}^{cm}\rangle = |e_{k+1}\rangle + \sqrt{1 + \epsilon_{k+1}} V_{k+1} \tilde{U}_{k+1} |e_k^{cm}\rangle \quad (11)$$

and the square of its norm $\epsilon_{k+1}^{cm} = \langle e_{k+1}^{cm} | e_{k+1}^{cm} \rangle$ obeys the recurrence relation $1 + \epsilon_{k+1}^{cm} = (1 + \epsilon_{k+1})(1 + \epsilon_k^{cm})$ since the elementary error vector $|e_{k+1}\rangle$, for which all previous ancillary particles have been disentangled, is orthogonal to the vector $V_{k+1} \tilde{U}_{k+1} |e_k^{cm}\rangle$. Thus,

$$1 + \epsilon_{k+1}^{cm} = \prod_{i=1}^{k+1} (1 + \epsilon_i). \quad (12)$$

3. Global error

After the choice of m disentanglers and m isometries, the reconstructed state is $|\phi\rangle = V_m^\dagger \tilde{U}_m^\dagger \dots V_1^\dagger \tilde{U}_1^\dagger |0\rangle^{\otimes m+1} |\eta_m\rangle$. Its difference to the actual experimental state $|\psi\rangle$ can be stated in terms of the (in) fidelity as

$$\begin{aligned} 1 - |\langle \phi | \psi \rangle|^2 &= 1 - 1 / (1 + \epsilon_m^{cm}) \\ &= 1 - 1 / \prod_{i=1}^m (1 + \epsilon_i). \end{aligned} \quad (13)$$

Practically, one is interested in guaranteeing that the reconstructed state is close to the experimental up to global error E , i.e., to guarantee that $1 - |\langle \phi | \psi \rangle|^2 \leq E$. Suppose that all error vectors are bounded, i.e. that for all step i , we have $\epsilon_i \leq \epsilon$. Inverting (13), it suffices that

$$\epsilon \leq (1 - E)^{-1/m} - 1 \simeq E/m$$

in the limit where the tolerable global error E is small. Thus, we see that *errors accumulate linearly* and that a precision inversely proportionnal to the number of disentanglers is sufficient to ensure a constant global error. Furthermore, statistics on the post-selection performed at each step allows to estimate each ϵ_k^{cm} and in particular ϵ_m^{cm} that gives direct access to the distance between the reconstructed and experimental states.

Finally, from this measurement data, one can estimate the error ϵ_i performed at each step in order to identify steps that have gone wrong. This information can be used to turn the scheme into an *adaptive* one. Suppose the error is particularly large for a given step. This might be due to an important amount of entanglement concentrated in one region of space, *e.g.* near a defect, which can be accounted for by increasing the MERA refinement parameter χ locally, i.e. by using disentanglers acting on a larger number of qubits. In principle, χ could be increased until the error is below some threshold.

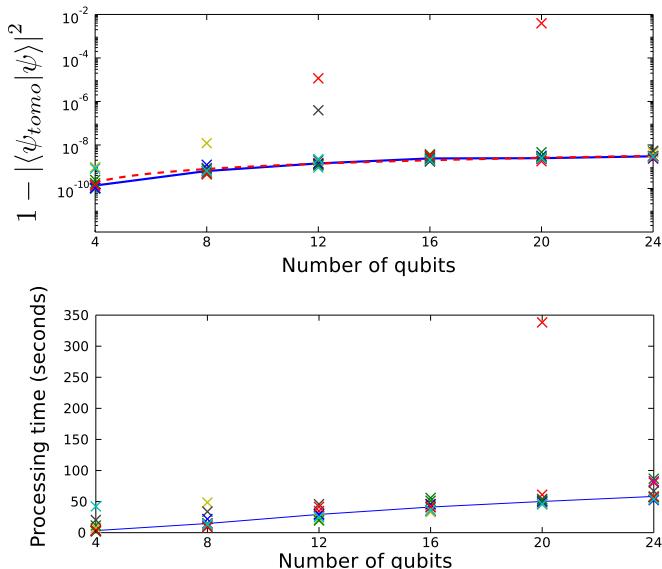


Figure 3: (top) Infidelity to the “experimental state”, *i.e.*, $1 - |\langle \psi_{\text{tomo}} | \psi \rangle|^2$ where $|\psi\rangle$ is a random MERA on n qubits and $|\psi_{\text{tomo}}\rangle$ is the state reconstructed from the MERA learning method using three sweeps. (bottom) Processing time (on a standard laptop) to perform MERA learning using three sweeps. Both figures exhibit 10 runs for each number of qubits $n \in \{8, 12, 16, 20, 24\}$. In both figures, each \times represents results for one random MERA. The full lines represent median for each number of qubits. The dashed line on the top figure is the linear approximation to the median. Notice that the numerical minimisation can fail to converge as illustrated by the atypical data points. For instance, for one of the 20-qubit MERA, the processing time was 338.3 seconds and the infidelity to the true state is large, $1 - |\langle \psi_{\text{tomo}} | \psi \rangle|^2 = 3.916 \times 10^{-3}$.

C. Numerical performance

1. Benchmarking results

We have performed numerical simulations to benchmark the performances of the MERA learning method. We have generated random MERA states—by picking each unitary gate in the circuit from the unitary group Haar measure—, simulated the experiment on those states, and use our algorithm to infer the initial MERA state. We did not introduce noise in measurements to simulate experimental errors since the error analysis indicates how those errors would build up.

As mentioned before, there is no guarantee that our minimization procedure converges to the true minimum, resulting in small imperfections in the reconstructed state. Figure (3, top) shows the distance between the reconstructed state and the actual state. As indicated by the dashed line, these results are in good agreement with a linear scaling of the error where the source of errors is due to finite machine precision and approximate minimisation of the objective function.

The inference algorithm’s complexity is dominated by

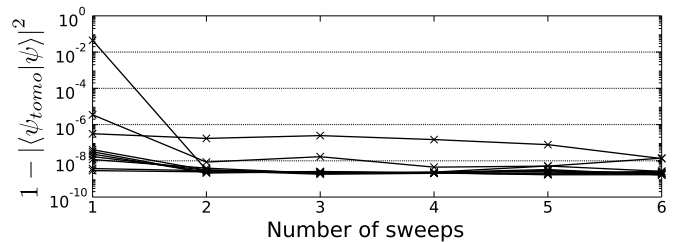


Figure 4: Infidelity to a 20 qubit state using a reconstructed method with a variable number of sweeps. Each line corresponds to a different random MERA.

the conjugate gradient descents, and therefore scales linearly with the number of disentanglers or the number of particles in the system. Figure (3, bottom) shows the actual runtime of the inference algorithm for different randomly chosen MERA states and of various sizes. Once again, we see a good agreement with a linear dependence with the system size. Systems of up to 24 qubits can easily be handled in a few minutes of computation and requires 1197 different measurement settings for each sweep of the 24 qubit system. This is to be contrasted with the 656,100 experiments needed to reconstruct the state of 8 qubits in [3] and the post-processing of the data that took approximately a week [27]. Additional sweeps allow the method to converge as showed on Fig. 4.

We also tested how our method behaved on a physical model, namely the 1D Ising model with transverse field at the critical point. The results obtained were coherent with what is expected from the approximation of the true ground state with a MERA with refinement parameter $\chi = 2$.

2. Possible improvements

Note the presence of isolated points on the graphs of Fig. 3 that achieve a lower fidelity and required a longer running time. These cases appear because the heuristic fails to find a global minimum. It appears that in some cases, a unitary transformation U_{23} meeting criterion (3) is not sufficient to guarantee that it will be possible to find subsequent disentanglers obeying (3). Put another way, *locally* minimising the objective function might not lead to a *global* optimum. Indeed, consider the following example. Let $|\psi\rangle$ be a MERA state whose first qubit is disentangled from the rest of the chain, *i.e.* $|\psi\rangle = |0\rangle|\phi\rangle$. The rank of the density matrix on the first two qubits is at most 2 and that remains true after *any* unitary is applied on qubits 2 and 3. Thus, any choice of disentangler minimises the objective function (3), including the identity, *i.e.*, applying no disentangler at all. However, suppose the state $|\phi\rangle$ on qubits 2 to n is highly entangled and that removing part of this entanglement between qubits 2 and 3 was crucial to be able to reconstruct its MERA description. In this case, applying the identity on qubits 2 and 3, even if locally optimal, was not globally opti-

mal. Hence, minimizing the objective function (3) seems to be necessary but not sufficient to successively identify all disentanglers.

Although our numerical simulations suggest that this situation is rather atypical, it is possible to overcome this problem by imposing additional constraint on the disentangler. For instance, one can demand that the second qubit be in a state as pure as possible, effectively minimizing the entanglement between the last qubit of one block and the first qubit of the next block. This corresponds to the following modified objective function

$$f(\tilde{\rho}_{12}[U]) = \sum_{k>2} \lambda_k + \epsilon \lambda_2 \quad (14)$$

i.e., we add a small perturbation that will only take action when the two smallest eigenvalues of $\tilde{\rho}_{12}[U_{23}]$ are very small and will further constrain the search. This slight modification solved the problematic situation we considered, and there exist many other heuristics to improve the method.

D. Trading unitary control for repeated measurements

For pedagogical reasons, we presented our learning method in a way that required disentanglers and isometries to be physically applied to the experimental state in order to unravel the circuit. In this section, we will show how to circumvent unitary control at the price of slightly more elaborate numerical processing and consuming more copies of the state. The main idea is to numerically simulate how measurements performed on the original, unaltered experimental system would be transformed if the unraveling circuit had been applied.

1. Simulating measurements on renormalized state

Recall that a MERA is an ansatz that corresponds to a renormalization procedure. Each renormalisation step maps a state to another one on fewer particles and schematically corresponds to a layer of the MERA circuit. Applying the first layer and removing the ancillary particles that have been (approximately) disentangled maps the experimental state ρ_0 on n particles to a state ρ_1 on fewer particles (see Fig 5). Recursively, this procedure constructs a sequence of states $\{\rho_\tau\}_\tau$.

To get from $\rho_{\tau-1}$ to ρ_τ , one can either perform this mapping *physically* by experimentally applying the gates corresponding to the MERA layer, or one can *compute* the function mapping $\rho_{\tau-1}$ to ρ_τ from the description of the gates. As in [17], define an ascending superoperator \mathcal{A} that maps an operator $O_{\tau-1}$ acting on layer $\tau-1$ to the an operator O_τ acting on the next layer τ

$$O_\tau = \mathcal{A}_\tau(O_{\tau-1}) \quad (15)$$

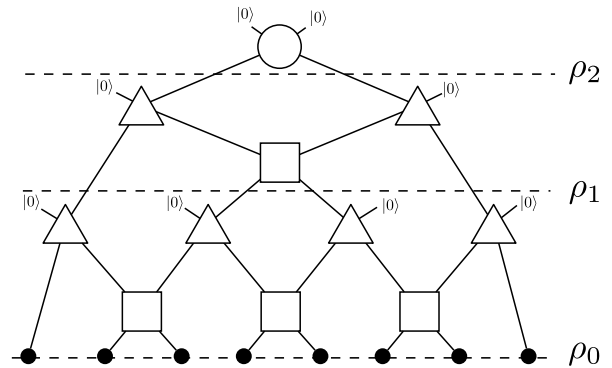


Figure 5: MERA as a renormalisation procedure that creates a sequence of states $\{\rho_\tau\}_\tau$.

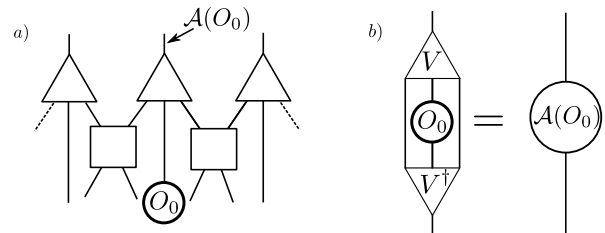


Figure 6: Ascending superoperator and renormalized observables for a ternary MERA. a) Ternary MERA with one site observable O_0 that is transformed into a renormalized observable $\mathcal{A}(O_0)$ on the renormalized state. b) Tensor contraction corresponding to the ascending superoperator \mathcal{A} .

such that

$$\text{Tr}[\rho_\tau \mathcal{A}_\tau(O_{\tau-1})] = \text{Tr}[\rho_{\tau-1} O_{\tau-1}]. \quad (16)$$

This recursively carries over to the experimental state ρ_0

$$\text{Tr}[\rho_\tau \mathcal{A}_\tau \circ \dots \circ \mathcal{A}_1(O_0)] = \text{Tr}[\rho_0 O_0]. \quad (17)$$

Thus, in order to extract information from a density matrix ρ_τ , one can measure the expectation value of several observables O_0^i on the density matrix ρ_0 . Measuring those observables will effectively amount to measuring the observables $O_\tau^i \equiv \mathcal{A}_\tau \circ \dots \circ \mathcal{A}_1(O_0^i)$ on the density matrix ρ_τ .

The ascending superoperator can be computed from the knowledge of the disentanglers and isometries. Its exact form depends on the physical support of the observable. For instance, for ternary MERA, we can restrict to ascending superoperator that only depends on the isometries of the MERA [22] (see Fig. 6). This is a simple example where an experimental observable on one particle is mapped to observable on one particle. More generally, observables on many sites will be ascended to observables on fewer sites. Any choice of observables is valid as long as the renormalized observables $\{O_\tau^i\}_i$ span the support of the reduced density matrix ρ_τ .

2. Overhead in the number of measurements

This procedure leads to an overhead in the total number of measurements because renormalized observables are less efficient at extracting information. Suppose (for clarity) that we measure Pauli observables $\{O_0^i\}_i$ on the experimental states. These observables are orthonormal for the Hilbert-Schmidt inner product and thus maximize information extraction. However, the renormalized observables $O_1^i \equiv \mathcal{A}_1(O_0^i)$ need not be orthonormal. Consider their Gram matrix $G_{ij} = \text{Tr} \left[O_1^i (O_1^j)^\dagger \right]$ which can be diagonalised by a unitary matrix Z . Its normalised eigenvectors $R_1^i = \frac{1}{\sqrt{\lambda_i}} \sum_j Z_{ij} O_1^j$ are orthonormal observables but cannot be directly measured because they do not correspond to simple observables on the experimental state, but instead to a linear combination of them. Thus, to reconstruct the density matrix $\rho_1 = \sum_i r_1^i R_1^i$, the expectation values $r_1^i = \text{Tr} \rho_1 R_1^i$ have to be computed by taking a linear combination of the expectation values $o_0^j \equiv \text{Tr} \rho_0 O_0^j$ on the experimental state

$$r_1^i = \frac{1}{\sqrt{\lambda_i}} \sum_j Z_{ij} \text{Tr} \rho_1 O_1^j = \frac{1}{\sqrt{\lambda_i}} \sum_j Z_{ij} o_0^j. \quad (18)$$

Due to a limited number of repeated measurements, estimation of each o_0^i will present a variance $\mathbb{V}(o_0^i)$. Suppose that measurements are repeated enough times to ensure that all variances are below a precision threshold, i.e., $\mathbb{V}(o_0^i) \leq \epsilon$. Since r_1^i is a linear combination of those measurements, it will have a variance $\mathbb{V}(r_1^i) = \frac{1}{\lambda_i} \sum_j |Z_{ij}|^2 \mathbb{V}(o_0^j) \leq \epsilon / \lambda_i$. Therefore, in order to ensure a precision ϵ on the estimate of r_1^i , this imprecision needs to be compensated by multiplying the number of repeated measurements by the *conditioning factor* λ_i^{-1} .

When scaling operators on τ layers, the conditioning factors for each layer will multiply (in the worst case) but we expect the conditioning for each layer to be a constant independent of system size. Thus, the total number of measurements will remain *polynomial* in the number of particles since there is only a *logarithmic* number of renormalisation layers.

We can make this argument rigorous for critical systems that exhibit scale-invariance, precisely the physical systems for which MERA was introduced. Due to scale-invariance, the ascending operator \mathcal{A}_τ will not depend on the index of the layer and we refer to it as the scaling superoperator \mathcal{S} [22]. Its diagonalization yields eigenvectors ϕ_α called scaling operators associated to eigenvalues μ_α . In [22], it was shown that those eigenvalues are related to the scaling dimensions Δ_α of the underlying conformal field theory (CFT) by $\Delta_\alpha = \log_3 \mu_\alpha$ where the basis of the log depends on the MERA type (here we consider a ternary MERA for clarity). Scaling operators ϕ_α can be used as observables to extract information about states in higher levels of the MERA. Indeed, one can simulate a measurement of $\mathcal{S}^\tau(\phi_\alpha)$ on ρ_τ by measuring the observable ϕ_α on ρ_0 . We can analyze the increase in the

number of measurements by distinguishing two sources of imprecision. First, to reconstruct ρ_τ one has to use a normalised operator $\phi_\alpha^{[\tau]} = 3^{\tau \Delta_\alpha} \mathcal{S}^\tau(\phi_\alpha)$ whose increased statistical fluctuations have to be compensated by performing additional measurements. Second, diagonalising the Gram matrix of the $\phi_\alpha^{[\tau]}$ will introduce another conditioning factor. However, this Gram matrix is independent of the layer since $G_{\alpha\beta}^{[\tau]} = \text{Tr} [\phi_\alpha^{[\tau]} \phi_\beta^{[\tau]}] = \text{Tr} [\phi_\alpha \phi_\beta]$. Thus, the conditioning factor for layer τ will be the product of a factor exponential in the number of layers and a constant factor coming from the orthonormalisation.

This modified scheme circumvents the need for unitary control, but loses some of the features of the original scheme. First, because the system is not physically disentangled, we cannot certify directly the fidelity of the reconstruction. Second, as explained in appendix A, the errors build up quadratically.

III. DISCUSSION

In this work, we have presented a tomography method that allows to efficiently learn the MERA description of a state by patching together tomography experiments on a few particles and using fast numerical processing. The method is heuristic but works very well in numerical simulations. A complete analytical understanding of how to find an optimal disentangler at each step would be desirable, but may well be intractable. With regards to experimental use, the method should be thought of as a proof of principle and is flexible enough to be adapted to accommodate many experimental constraints.

One issue of fundamental interest raised by our work is the relationship between the numerical tractability of a variational class of states and the ability to learn efficiently the variational parameters. In order to be interesting, a variational class of states must not only be described by a small number of parameters, but also allow for the efficient numerical computation of quantities of interest, such as the energy of the system, correlation functions, or more generally expectation values of local observables. On its own, an efficient representation is of limited computational usefulness. For instance, the Gibbs state or thermal state of a local Hamiltonian is described by a few parameters — a temperature and a local Hamiltonian — but does not allow to extract physical quantities of interest efficiently. Another example is the variational class of projected entangled pair states or PEPS [28], the generalization of MPS to systems in more than one dimension. While PEPS have been instrumental in better understanding of quantum many-body systems, they are in general intractable numerically [29].

Is there a relation between numerical tractability and efficient tomography? The method presented in [15] to learn a MPS from local measurements made explicit use of the energy minimization algorithm for MPS; namely DMRG [30]. This example suggests that numerical

tractability could imply that learning the variational parameters is possible. In that regard, MERA are intriguing states because they live at the frontier of tractability. Indeed, in more than 1 dimension, MERA states are a subclass of PEPS [31] with a bond dimension independent of system size [32]. While the computation of expectation values of local observables is believed to be intractable for PEPS, it is efficient for MERA. In one dimension, MERA can be seen as MPS if one allows the bond dimension to grow *polynomially* with the size of the system (while MPS are usually required to have a *constant* bond dimension). Thus, while MPS manipulations typically have a computational cost linear in the number of particles, 1D-MERA manipulations have a computational cost which is superlinear (but yet polynomial).

Beyond MPS and MERA, one could consider states obtained from a quantum circuit where the positions of

the gates are known and try to identify those gates. An interesting question is then to characterize what topology of circuits makes it possible to learn gates efficiently. This could lead to formal methods for the testing and verification of quantum hardware.

Acknowledgments

OLC acknowledges the support of the Natural Sciences and Engineering Research Council of Canada (NSERC) through a Vanier scholarship. OLC wishes to thank Andy Ferris for stimulating discussions and sharing numerical data on scale-invariant MERAs. DP acknowledges financial support by the Lockheed Martin Corporation.

-
- [1] K. Vogel and H. Risken, Phys. Rev. A **40**, 2847 (1989).
 [2] S. Das Sarma, G. Gervais, and X. Zhou, Phys. Rev. B **82**, 115330 (2010).
 [3] H. Häffner, W. Hänsel, C. F. Roos, J. Benhelm, D. Chekhal Kar, M. Chwalla, T. Körber, U. D. Rapol, M. Riebe, P. O. Schmidt, et al., Nature **438**, 643 (2005).
 [4] J. T. Barreiro, P. Schindler, O. Gühne, T. Monz, M. Chwalla, C. F. Roos, M. Hennrich, and R. Blatt, Nature Physics **6**, 1 (2010).
 [5] L. DiCarlo, J. M. Chow, J. M. Gambetta, L. S. Bishop, B. R. Johnson, D. I. Schuster, J. Majer, A. Blais, L. Frunzio, S. M. Girvin, et al., Nature **460**, 240 (2009).
 [6] L. DiCarlo, M. D. Reed, L. Sun, B. R. Johnson, J. M. Chow, J. M. Gambetta, L. Frunzio, S. M. Girvin, M. H. Devoret, and R. J. Schoelkopf, arXiv 1004.4324 (2010).
 [7] S. Filipp, P. Maurer, P. Leek, M. Baur, R. Bianchetti, J. Fink, M. Göppl, L. Steffen, J. Gambetta, a. Blais, et al., Phys. Rev. Lett. **102**, 1 (2009).
 [8] H. Mikami, Y. Li, K. Fukuoka, and T. Kobayashi, Phys. Rev. Lett. **95**, 2 (2005).
 [9] K. Resch, P. Walther, and a. Zeilinger, Phys. Rev. Lett. **94** (2005).
 [10] I. Affleck, T. Kennedy, E. H. Lieb, and H. Tasaki, Phys. Rev. Lett. **59**, 799 (1987).
 [11] M. Fannes, B. Nachtergaele, and R. F. Werner, Commun. Math. Phys. **144**, 443 (1992).
 [12] G. Vidal, Phys. Rev. Lett. **91**, 12 (2003).
 [13] G. Vidal, Phys. Rev. Lett. **93**, 1 (2004).
 [14] F. Verstraete and J. Cirac, Phys. Rev. B **73** (2006).
 [15] M. Cramer, M. Plenio, S. Flammia, R. Somma, D. Gross, S. Bartlett, O. Landon-Cardinal, D. Poulin, and Y. Liu, Nature Communications **1**, 149 (2010).
 [16] G. Vidal, Phys. Rev. Lett. **101**, 1 (2008).
 [17] G. Evenbly and G. Vidal, Phys. Rev. B **79**, 144108 (2009).
 [18] L. Cincio, J. Dziarmaga, and M. Rams, Phys. Rev. Lett. **100**, 2 (2008).
 [19] M. Aguado and G. Vidal, Phys. Rev. Lett. **100**, 1 (2008).
 [20] G. Evenbly, R. N. C. Pfeifer, V. Picó, S. Iblisdir, L. Tagliacozzo, I. P. McCulloch, and G. Vidal, Phys. Rev. B **82**, 161107 (2010).
 [21] S. Montangero, M. Rizzi, V. Giovannetti, and R. Fazio, Phys. Rev. B **80**, 2 (2009).
 [22] R. Pfeifer, G. Evenbly, and G. Vidal, Phys. Rev. A **79**, 2 (2009).
 [23] R. König and E. Bilgin, Phys. Rev. B **82**, 1 (2010).
 [24] R. Pfeifer, P. Corboz, O. Buerschaper, M. Aguado, M. Troyer, and G. Vidal, Phys. Rev. B **82**, 1 (2010).
 [25] G. Vidal, arXiv **0707.1454v2** (2008).
 [26] M. P. da Silva, O. Landon-Cardinal, and D. Poulin, Phys. Rev. Lett. **107**, 210404 (2011).
 [27] R. Blume-Kohout, New J. Phys. **12**, 043034 (2010).
 [28] F. Verstraete, V. Murg, and J. Cirac, Advances in Physics **57**, 143 (2008).
 [29] N. Schuch, M. M. Wolf, F. Verstraete, and J. I. Cirac, Phys. Rev. Lett. **98**, 140506 (2007).
 [30] U. Schollwöck, Rev. Mod. Phys. **77**, 259 (2005).
 [31] F. Verstraete and J. Cirac, arXiv:cond-mat/0407066. (2004).
 [32] T. Barthel, M. Kliesch, and J. Eisert, Phys. Rev. Lett. **105**, 6 (2010).

Appendix A: Error analysis without post-selection

The modified scheme that circumvents the need of unitary control modifies the error propagation. Indeed, the scaling of the overall error increases since the error at each step will depend on previous errors. Essentially, to find the optimal disentangler, the algorithm will not receive the perfect state $|\eta_k\rangle$ (see eq. (8)) but the state $\frac{1}{1+E_k^{cm}}|\eta_k\rangle + \frac{E_k^{cm}}{1+E_k^{cm}}|E_k^{cm}\rangle$ where $|E_k^{cm}\rangle$ is a subnormalised error vector resulting from the accumulation of all previous errors whose square norm is $E_k^{cm} \equiv \langle E_k^{cm} | E_k^{cm} \rangle$. Thus, the numerical minimisation returns a unitary that is not the perfect disentangler.

In the degenerate case —when there are many unitaries reaching roughly the same minimum value of the objective function—, this might change the disentangling unitary drastically. Indeed, we note that the existence of

degenerate local minima affects both of our tomography methods, the one with and the one without unitary control of the system. In such degenerate cases, exploring many local minima by selecting random initial guesses could get around the problem. However, it is likely that these instances are intrinsically hard and that our algorithm does not converge to the right answer in those cases, c.f. the atypical data points on Fig. 3.

In the non-degenerate case, we can argue that the accumulation of errors would be *quadratic* in the number of particles. We proceed in three steps. First, we analyze how the modification of the input state will affect the disentangling unitary returned by the algorithm. Second, we evaluate how this imperfect disentangler impacts the error propagation. Third, we bound the error to show the quadratic scaling.

Our algorithm returns the unitary $\tilde{U} = e^{i\tilde{H}}$ that minimizes the objective function (3) for a given state ρ . If we don't post-select on the ancillary particles being disentangled, this minimization is not performed on the the perfect state $\rho_0 = |\eta_k\rangle\langle\eta_k|$ but rather on the state $(1-\varepsilon)\rho_0 + \varepsilon\sigma$ where $\varepsilon = \frac{E_k^{cm}}{1+E_k^{cm}}$ and $\sigma = |E_k^{cm}\rangle\langle E_k^{cm}|$. We want to know how much $\tilde{U} = \arg \min_U f(U, \rho)$ changes when ρ changes. Using the chain rule, we formally write $\frac{\partial \tilde{U}}{\partial \rho} = \frac{\partial \tilde{U}}{\partial f} \frac{\partial f}{\partial \rho}$. The first term quantifies how much \tilde{U} changes when the objective function changes for a given ρ . In the non-degenerate case, we expect this term to be bounded in norm by a Lipschitz constant η . The second term evaluates how the objective function changes when going from ρ_0 to $(1-\varepsilon)\rho_0 + \varepsilon\sigma$. Recalling that the objective function is a sum of eigenvalues and using non-degenerate perturbation theory, this term is going to be proportional to ε . Thus, instead of $\tilde{U} = e^{i\tilde{H}}$, the minimization algorithm returns $e^{i(\tilde{H} + \varepsilon\eta A)} \approx W\tilde{U}$ where $W = e^{i\varepsilon\eta A}$.

As a consequence, eq. (10) is modified to read

$$W_{k+1} \frac{|0\rangle^{\otimes k+1} |\eta_{k+1}\rangle + |E_{k+1}^{cm}\rangle}{\sqrt{1 + \epsilon_{k+1}^{cm}}} = e^{i\theta} \frac{|0\rangle^{\otimes k+1} |\eta_{k+1}\rangle + |E_{k+1}^{cm}\rangle}{\sqrt{1 + E_{k+1}^{cm}}}. \quad (\text{A1})$$

Taking into account the anomalous unitary W , we get

$$1 + E_{k+1}^{cm} = 1 + \epsilon_{k+1}^{cm}/\beta^2 = (1 + \epsilon_{k+1})(1 + E_k^{cm})/\beta^2 \quad (\text{A2})$$

where $\beta^2 = |\langle \eta_{k+1} | \langle 0 |^{\otimes k+1} W | 0 \rangle^{\otimes k+1} | \eta_{k+1} \rangle|^2 = |\langle W \rangle|^2$. Using $W = e^{i\varepsilon\eta A}$, calculations show that

$$\beta^2 = 1 - \varepsilon^2 \eta^2 (\langle A^2 \rangle - \langle A \rangle^2) = 1 - \varepsilon^2 \eta^2 \Delta^2 \quad (\text{A3})$$

where the variance Δ^2 of A with respect to state $|0\rangle^{\otimes k+1} |\eta_{k+1}\rangle$ appears. Recalling that $\varepsilon = \frac{E_k^{cm}}{1+E_k^{cm}}$, one gets

$$\beta^2 = \frac{(1 + E_k^{cm})^2 - (E_k^{cm})^2 \eta^2 \Delta^2}{(1 + E_k^{cm})^2} \geq \frac{1}{(1 + E_k^{cm})^2} \quad (\text{A4})$$

for any E_k^{cm} if $\eta^2 \Delta^2 \leq 1$ or for small E_k^{cm} otherwise.

Thus, the error magnitude E_{k+1}^{cm} obeys the recurrence relation

$$\begin{aligned} 1 + E_{k+1}^{cm} &\leq (1 + E_k^{cm})^3 (1 + \epsilon_{k+1}) \\ &\leq (1 + \epsilon_1)^{3^k} \dots (1 + \epsilon_{k+1}). \end{aligned}$$

Assuming that the error at each step is bounded $\epsilon_k \leq \epsilon$, the total error scales as

$$E_m^{cm} \leq \frac{3}{2} m^2 \epsilon. \quad (\text{A5})$$

Appendix B: Comparing a reconstructed MERA to a predicted MERA

In this section, we describe a polynomial algorithm to contract two MERA states, thus allowing to compute their fidelity. This algorithm is of practical interest for comparing a MERA whose parameters have been identified experimentally using our method to a predicted MERA state –found by numerical optimisation for instance. Notice that contracting two different MERA states also allows to compute expectation values of tensor product of local observables $\bigotimes_i A_i$ since it suffices to contract the original state $|\psi\rangle$ and the modified state $|\phi\rangle = \bigotimes_i A_i |\psi\rangle$, which is also a MERA state.

Defining a method to contract two MERA states is equivalent to giving a prescription on how to sequentially contract the tensor network resulting from joining two MERA states. Recall that contracting two tensors $(M)_{i_a j_b}$ and $(N)_{k_b \ell_c}$ to obtain $T_{i_a \ell_c} = \sum_{j_b} M_{i_a j_b} N_{j_b \ell_c}$ has a computational cost of $a \times b \times c$ where a is the number of values that the index i_a can take b and c are defined in the same way with respect to j_b and ℓ_c . In a tensor network, every tensor is usually represented with a number of bonds that each represent an index that has the same maximal number of possible values. For a MERA, this maximal bond dimension is usually denoted by χ .

The main idea to contract efficiently two MERA states is essentially to turn them into two MPS before contracting them. We look at the MERA circuit as having $n/2$ columns of gates vertically and $\log_\chi n - 1$ renormalisation layers horizontally. The sequence of contraction is to sequentially contract every tensor in the leftmost column to create a tensor with a large number of bonds that will then contract with every tensor in the next column. The maximal number of bonds that this leftmost tensor will have throughout the contraction of the network is given by the maximal number of bonds that are opened when taking a vertical cut in the tensor network. For a single MERA, cutting through each of the $\log_\chi n - 1$ layer opens up two bonds, one for the rightmost incoming edge of the isometry and one for the outgoing edge of the isometry. Thus, for the contraction of two MERAs, the maximum number of bonds for a vertical cut is bounded by $\max \# = 2 \times 2 \times \log_\chi n = 4 \log_\chi n$, which is verified numerically (see top of Fig. 7). Since at every contraction

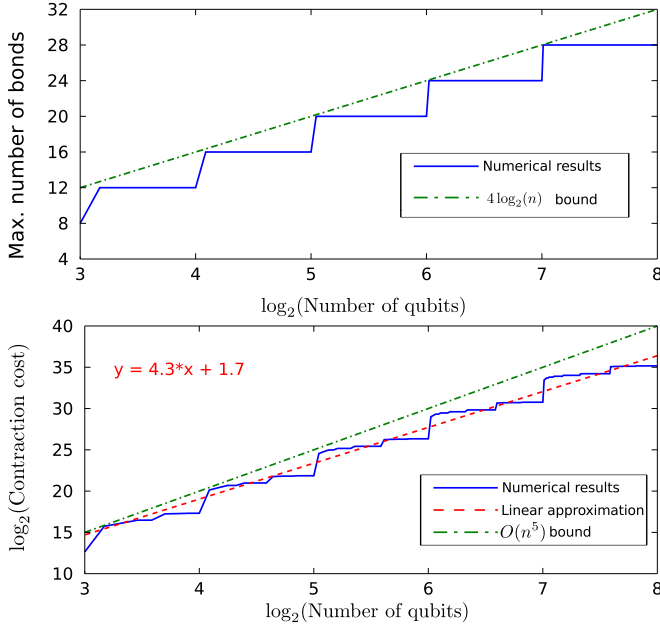


Figure 7: (top) Maximum number of bonds during the contraction procedure as a function of the logarithm of the number of qubits n . Numerical results (solid blue line) are consistent with the expected bound of $4\log_2 n$. (bottom) Contraction cost C as a function of the number n of qubits on a logscale. Numerical results (solid blue line) are consistent with the $O(n^5)$ bound (dot dashed green line) but linear approximation (dashed red line) indicate that the cost scales like a smaller power of n , namely $C \simeq n^{4.3}$.

step, the leftmost tensor with a large number of bonds contract with another tensor that has at most two bonds in addition to the ones being contracted, the maximum cost of one contraction is $\chi^{\max} \# \chi^2 = \chi^2 n^4$. Finally, there are $O(n)$ disentanglers and isometries to contract so the total cost of contracting the network is bounded by $O(n^5)$. Actual numerical simulations show that this bound is probably not tight (see bottom of Fig. 7).